iScience

CellPress
OPEN ACCESS

Article

Inhibition of Phase Segregation in Cesium Lead Mixed-Halide Perovskites by B-Site Doping

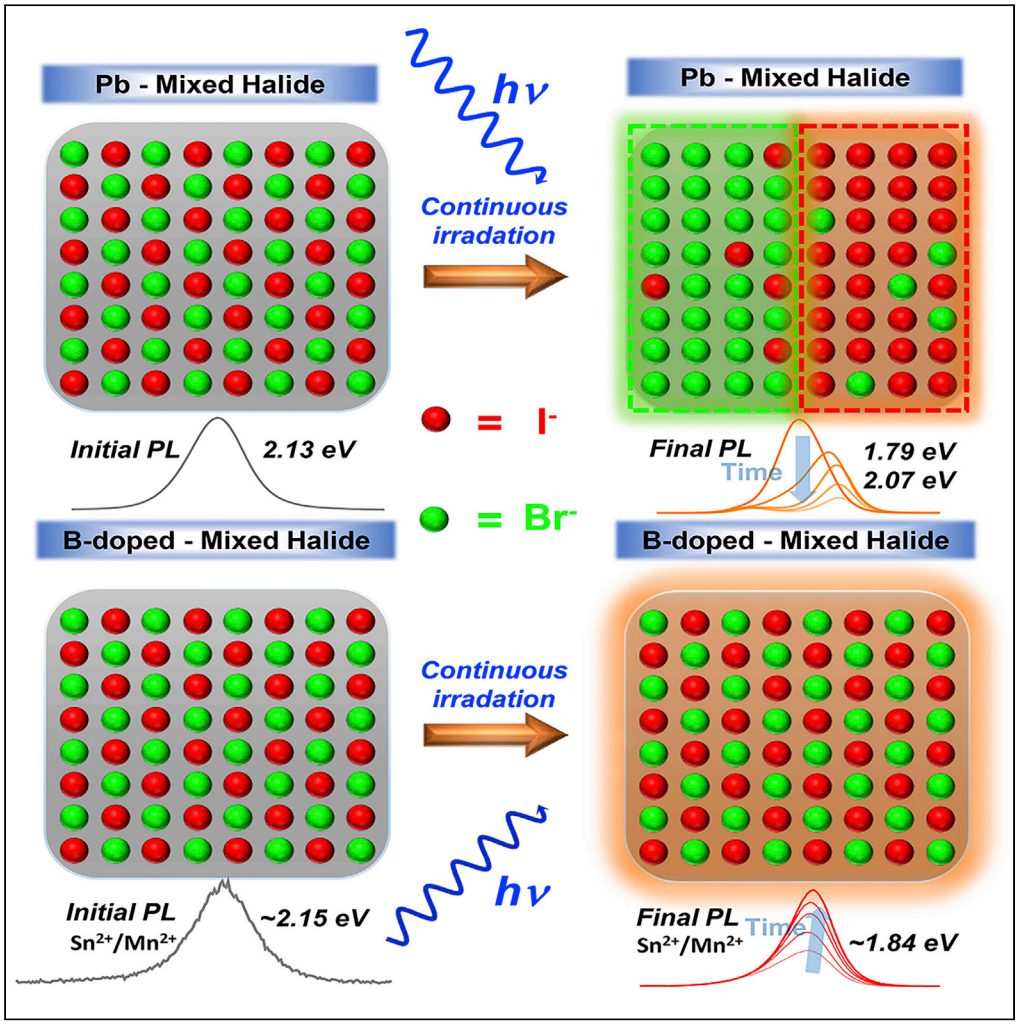

Daocheng Hong, Peiyang Zhao, Yu Du, ..., Zhihong Wei, Zhong Jin, Yuxi Tian

jinzhong@nju.edu.cn (Z.J.)
tyx@nju.edu.cn (Y.T.)

HIGHLIGHTS

Phase segregation process of perovskite materials can be real-time monitored by PL

Sn^{2+}/Mn^{2+} doping can significantly improve the phase stability of $CsPbI_xBr_{3-x}$

Mn^{2+} doping brings $CsPbI_xBr_{3-x}$ higher tolerance to oxygen and moisture

Hong et al., iScience 23, 101415
August 21, 2020
https://doi.org/10.1016/j.isci.2020.101415

iScience

CellPress
OPEN ACCESS

Article

Inhibition of Phase Segregation in Cesium Lead Mixed-Halide Perovskites by B-Site Doping

Daocheng Hong,[1,2] Peiyang Zhao,[1] Yu Du,[1] Cheng Zhao,[1] Yuren Xia,[1] Zhihong Wei,[1] Zhong Jin,[1,*] and Yuxi Tian[1,3,*]

SUMMARY

The emergence of all-inorganic halide perovskites has shown great potential in photovoltaic and optoelectronic devices. However, the photo-induced phase segregation in lead mixed-halide perovskites has severely limited their application. Herein, by real-time monitoring the photoluminescence (PL) spectra of metal mixed-halide perovskites under light irradiation, we found that the photo-induced phase transition can be significantly inhibited by B-site doping. For pristine mixed-halide perovskites, an intermediate phase of $CsPbBr_xI_{3-x}$ can only be stabilized under low excitation power. After introducing Sn^{2+} ions, such intermediate phase can be stabilized in nitrogen atmosphere under high excitation power and phase segregation can be started after the exposure in oxygen due to oxidization of Sn^{2+}. Replacing Sn^{2+} by Mn^{2+} can further improve the intermediate phase's tolerance to oxygen proving that B-site doping in perovskites structure by Sn^{2+} or Mn^{2+} could effectively minimize the light-induced phase segregation and promote them to serve as promising candidates in photovoltaic and light-emitting devices.

INTRODUCTION

Photovoltaic and optoelectronic devices composed of organic-inorganic hybrid perovskites have achieved incredible development during the past 10 years (Green et al., 2014; Snaith, 2013; Tan et al., 2014). The power conversion efficiency of perovskite solar cells has skyrocketed from 3.8% to 25.2% (Bi et al., 2015; Jiang et al., 2017, 2018; NREL, 2020; Ono et al., 2018; Wu et al., 2016). Meanwhile, the external quantum efficiency of perovskite-based light-emitting diodes (LEDs) has also been reported to exceed 20% (Cao et al., 2018; Lin et al., 2018). However, the major challenge that remained for these materials is the poor stability, which mainly originated from the non-negligible vapor pressure of the organic moieties and their complex interactions with the moisture in air (Han et al., 2015; Leijtens et al., 2015; Mosconi et al., 2015). To improve stability, substituting the organic cations by inorganic Cs^+ ions has been regarded as an effective method. Cs-based perovskites solar cells have been reported to show high stability against humidity and heat (Liang et al., 2016; Wang et al., 2018).

Nevertheless, there are still some drawbacks limiting the application of Cs-based all-inorganic perovskites. One of them is the large band gap (~2.3 eV for $CsPbBr_3$), which only allows $CsPbBr_3$ to absorb light from the UV region. And most part of the visible light in the solar spectrum cannot be utilized, which seriously limits the improvement of power conversion efficiency (Chang et al., 2016; Duan et al., 2018; Liang et al., 2016). Comparatively, $CsPbI_3$ owns a narrower band gap (~1.73 eV), leading to a wider light absorption range. However, the most ideal black-$CsPbI_3$ (cubic phase) is thermodynamically less favorable and tends to spontaneously turn into the orthorhombic phase δ-$CsPbI_3$ under ambient condition (Eperon et al., 2015). Mixed-halide perovskite $CsPbIBr_2$ with a narrower band gap than $CsPbBr_3$ and a better thermodynamic stability than $CsPbI_3$ is proposed to be a better choice of light absorbers. Unfortunately, light-induced halide segregation still cannot be avoided in these all-inorganic mixed-halide perovskite absorbers (Beal et al., 2016; Hoke et al., 2015; Noh et al., 2013; Zhang et al., 2019). Several previous studies have documented that the engineering of band gap in perovskites by interchanging bromide and iodide did not yield a corresponding increase in photo-conversion efficiency because of light-induced halide phase segregation (Hoke et al., 2015).

[1]Key Laboratory of Mesoscopic Chemistry of MOE, School of Chemistry and Chemical Engineering, Nanjing University, Nanjing, Jiangsu 210023, China

[2]Key Laboratory for Advanced Technology in Environmental Protection of Jiangsu Province, Yancheng Institute of Technology, Yancheng 224051, China

[3]Lead Contact

*Correspondence: jinzhong@nju.edu.cn (Z.J.), tyx@nju.edu.cn (Y.T.)

https://doi.org/10.1016/j.isci.2020.101415

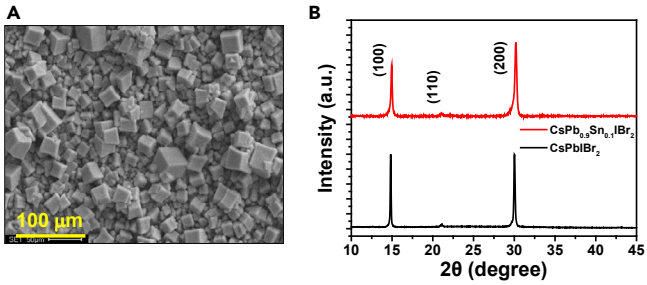

Figure 1. Characterization of the Perovskite Films

(A) Morphology of $CsPb_{0.9}Sn_{0.1}IBr_2$ film taken by SEM. The scale bar is 100

(B) XRD pattern of $CsPb_{0.9}Sn_{0.1}IB_{r2}$ film (red solid line) and $CsPbIBr_2$ film (black solid line).

Recently, it is reported that the partial substitution of Pb by Sn in $CsPbIBr_2$ perovskite can not only help to improve the efficiency but also show good long-term stability in photovoltaic devices (Li et al., 2018b; Liang et al., 2017). To find out how the exceptional improvement happens in Sn-doped all-inorganic halide mixed perovskites, we prepared $CsPbIBr_2$ and $CsPb_{0.9}Sn_{0.1}IBr_2$ perovskites and made a comparison between them by monitoring their real-time photoluminescence (PL) spectrum. Under continuous light irradiation, we observed that the phase-segregation of $CsPbIBr_2$ happened rapidly, while $CsPb_{0.9}Sn_{0.1}IBr_2$ can be stabilized at an intermediated state, which was consistent with the metastable $CsPbBr_xI_{3-x}$ formed under low excitation power density. With the further oxidization of Sn^{2+} ions in $CsPb_{0.9}Sn_{0.1}IBr_2$ material, the phase-segregation started again, verifying that the Sn^{2+} doping in mixed-halide perovskites can effectively minimize the light-induced phase segregation. Substitution of Sn^{2+} by Mn^{2+} in mixed-halide perovskites was further proved to be able to increase the intermediated state's tolerance to oxygen indicating that B-site doping is an effective way to promote the performance of the mixed-halide perovskite materials as photovoltaic and light-emitting devices.

RESULTS AND DISCUSSION

Material Characteristics of Sn^{2+}-Doped Perovskites

The morphology of as-prepared $CsPb_{0.9}Sn_{0.1}IBr_2$ films was characterized by scanning electron microscopy (SEM), as shown in Figure 1A. The corresponding elemental mappings measured by energy-dispersive X-ray spectroscopy (EDX) were also taken and presented in Figure S1. The results of the quantitative analysis in Table S1 demonstrate that the compositions in the film are in agreement with $CsPb_{0.9}Sn_{0.1}IBr_2$. As shown in Figure 1B, X-ray diffraction (XRD) pattern displays several peaks corresponding to (100), (110), and (200) planes, respectively, confirming the crystal structure is based on perovskite phase (Li et al., 2018b; Liang et al., 2017). The angles in $CsPb_{0.9}Sn_{0.1}IBr_2$ films (14.96°, 21.07°, 30.20°) are slightly larger than those in $CsPbIBr_2$ films (14.84°, 20.99°, 30.08°) indicating the shrinkage of the lattice after the doping of Sn^{2+} at the B site of the crystal structure. This result is in good agreement with the relative smaller ionic size of Sn^{2+} than Pb^{2+}.

Real-Time PL Variations of $CsPb_{0.9}Sn_{0.1}IBr_2$ and $CsPbIBr_2$ Films

We first measured the PL spectra of $CsPbIBr_2$ and $CsPb_{0.9}Sn_{0.1}IBr_2$ films under N_2 atmosphere with a 450-nm-wavelength laser and with the power density of 5 W/cm^2. As shown in Figure 2A, the initial PL spectrum of $CsPb_{0.9}Sn_{0.1}IBr_2$ showed a single peak with a maximum value at 576 nm (the inset of Figure 2A). With continuous light irradiation, the PL intensity significantly increased and the maximal position shifted to 676 nm within 10 min (Figures 2A and 2B), which might be caused by the photo-induced halide ions redistribution processes, similar to that in $MAPbBr_xI_{3-x}$ (Hoke et al., 2015), due to the lattice mismatch with different halide anion radius in fresh $CsPb_{0.9}Sn_{0.1}IBr_2$ samples. Also, the variation of the FWHM of the PL spectra indicates the transition process from a single PL peak to another one (Figure 2C). Then, the PL spectra kept stable and the intensity continuously increased for more than 100 times compared with the initial intensity (the inset of Figure 2B). The enhanced PL intensity has been widely reported, which could be due to two reasons: (1) energy transfer from large band gap phase to the newly formed stable low-energy phase, which has higher quantum yield; (2) passivation of the quenching defects by optimization of the crystal structure. Both of them can also correspond to the reported performance improvement in photovoltaic devices (Stranks, 2017). The PL emission of $CsPbIBr_2$ film also showed a single peak with maximum

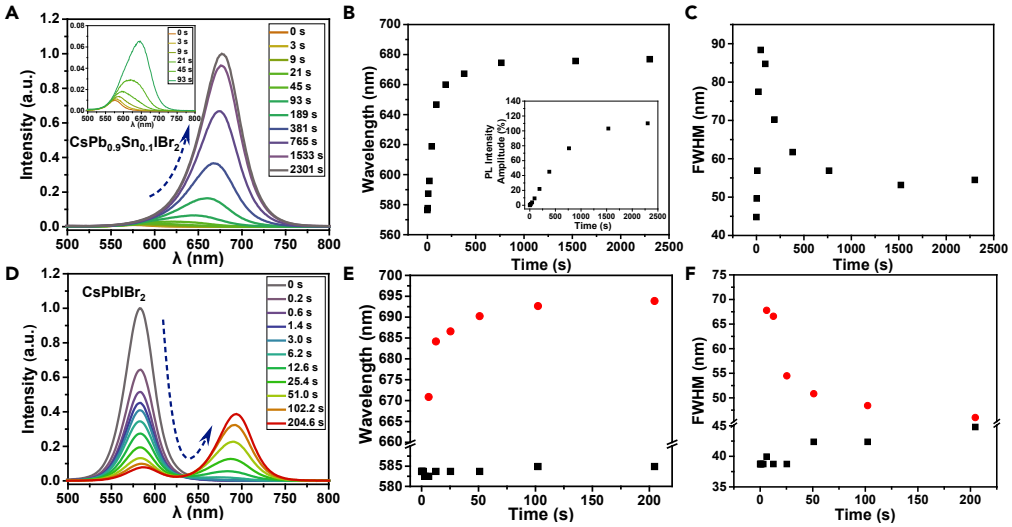

Figure 2. Real-Time PL Monitoring of $CsPb_{0.9}Sn_{0.1}IBr_2$ Films

(A) PL variations of $CsPb_{0.9}Sn_{0.1}IBr_2$ film under continuous irradiation. The inset in (A) shows the PL variation during the first 100 s in detail.

(B) PL peak wavelength in (A) varied as irradiation time. The inset in (B) shows the variation of PL intensity amplitude under continuous irradiation. The amplitude is calculated by $(I - I_0)/I_0(I\text{-}I_0)I_0$, in which I_0 indicates the initial PL intensity and I indicates the varied PL intensity.

(C) The full width at half maximum (FWHM) of the PL spectra in (A) varied as irradiation time.

(D) PL variations of $CsPbIBr_2$ under continuous irradiation.

(E) PL peak wavelength in (D) varied as irradiation time.

(F) The full width at half maximum (FWHM) of the PL spectra in (D) varied as irradiation time. Both samples were excited by a 450-nm laser excitation with a power density of 5 W/cm^2, and the PL measurements were taken under nitrogen atmosphere.

value around 584 nm at the initial time (Figure 2D). However, under continuous light irradiation, the PL intensity gradually decreased and a new peak appeared (Figure 2E) which can also be proved from the evaluation of PL FWHM (Figure 2F). A clear intensity decrease of the initial PL peak and a clear intensity increase of the new peak without spectral shift can be observed, indicating a phase transition process. The transition process stopped after 100 s with the final PL spectrum containing two peaks locating at 584 and 694 nm, respectively. These two peaks are proposed to be corresponding to bromide-rich phase and iodine-rich phase (Hoke et al., 2015) formed by the photo-induced phase-segregation behaviors (Slotcavage et al., 2016). Such fast phase segregation process in $CsPbIBr_2$ verifies that the lead mixed-halide perovskite is in a dynamically unfavorable state as reported (Bischak et al., 2017; Brivio et al., 2016). The PL enhancement and the single peak featured PL spectra of $CsPb_{0.9}Sn_{0.1}IBr_2$ suggests the formation of a stable phase, which is different from either the bromide-rich phase or the iodine-rich phase, as discussed below. As well known, PL properties of the perovskites are correlated to many factors including crystal structure (Klug et al., 2017), atmospheres (Fang et al., 2016; Galisteo-López et al., 2015; Tian et al., 2015), and degradation (Matsumoto et al., 2015). Since both PL variations were first taken under N_2 atmosphere, they should be free from the interactions between atmospheres and crystals. In addition, these measurements were performed under the same experimental conditions except the difference in the sample. That is to say, the difference of the PL properties between $CsPbIBr_2$ and $CsPb_{0.9}Sn_{0.1}IBr_2$ can be only due to the doping of Sn^{2+} ions. Therefore, we can conclude that the substitution of partial Pb^{2+} in $CsPbIBr_2$ with Sn^{2+} ions can successfully prevent it from segregating into two different phases under light soaking.

Because the stable PL emission of $CsPb_{0.9}Sn_{0.1}IBr_2$ films located just between the PL emissions of bromide-rich regions and iodine-rich regions in $CsPbIBr_2$ films, it must be a stable phase with the content of mixed-halide $CsPb_{0.9}Sn_{0.1}I_xBr_{3-x}$. Another evidence for this conclusion is that the spectrum of $CsPb_{0.9}Sn_{0.1}I_3$ phase should locate at a longer wavelength than $CsPbI_3$ due to the doping of Sn^{2+}(Hao et al., 2014). Actually, this mixed-halide phase has also been observed in $CsPbI_xBr_{3-x}$ (Slotcavage et al., 2016). We did not observe the intermediate state during the phase segregation process of $CsPbIBr_2$ films, possibly owing to the faster phase transition under high excitation power density. We thus rechecked the phase transition process of

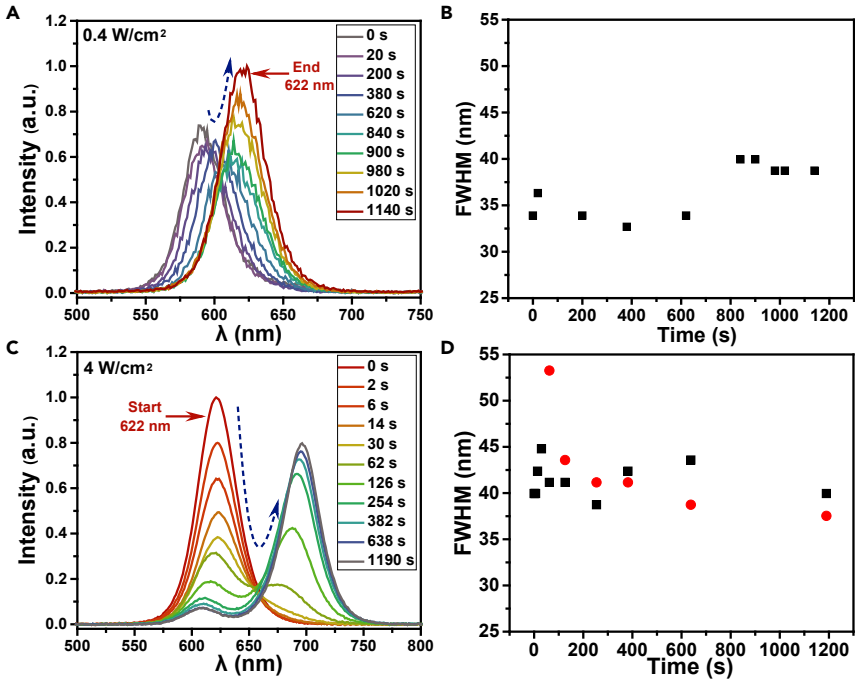

Figure 3. Real-Time PL Monitoring of $CsPbIBr_2$ Films

(A) PL variations of $CsPbIBr_2$ film under the excitation power density of 0.4 W/cm^2.

(B) The FWHM variation of the PL spectra in (A).

(C) PL variation of $CsPbIBr_2$ film under the excitation power density of 4 W/cm^2.

(D) The FWHM variation of the PL spectra in (C). The PL emissions in (A) and (C) were collected from the same location, the low-power excitation in (A) was first measured, and then the high-power excitation in (C) was measured after the low-power excitation was turned off.

$CsPbIBr_2$ films with a low excitation power density of 0.4 W/cm^2 in order to slow down the halide ions migration processes. As shown in Figure 3A, the PL emission started from 580 nm and redshifted to 622 nm. The stable FWHM in Figure 3B also indicates there is only one emission peak. That is to say, with low excitation power density, the halide redistribution process was successfully slowed down and could form an intermediate mixed-halides state ($CsPbI_xBr_{3-x}$). Such mixed-halides state was quite stable unless higher excitation power density was applied. As shown in Figure 3C and 3D, under a higher excitation power density of 4 W/cm^2, fast phase separation process happened, similar to the results shown in Figure 2D. The single peak located at 622 nm, which is stabilized under low power excitation (0.4 W/cm^2) proved the formation of the intermediate state ($CsPbI_xBr_{3-x}$) during the phase segregation process, which was very similar to the stable PL emission in $CsPb_{0.9}Sn_{0.1}IBr_2$. The redshifted PL emission in $CsPb_{0.9}Sn_{0.1}IBr_2$ intermediate state compared with that in $CsPbIBr_2$ is consistent with the fact that the occupation of Sn^{2+} ions in B sites of perovskite structure can decrease the conduction band minimum and make the band gap narrower (Brandt et al., 2015). The difference is that the peak position of PL emission in $CsPb_{0.9}Sn_{0.1}IBr_2$ film would keep stable, whereas that in $CsPbIBr_2$ film would start to separate into two peaks under high excitation power. In other words, the doping of Sn^{2+} ions in lead mixed-halide perovskites can effectively stabilize the intermediate state induced by light irradiation. The increased PL intensity of the intermediate state in $CsPb_{0.9}Sn_{0.1}IBr_2$ indicates its high tolerance properties to photo-excitation, which can also explain the significantly improved long-term stability relative to lead mixed-halide perovskites (Niezgoda et al., 2017; Yang et al., 2016). In principle, doping of Sn^{2+} ions in B sites will significantly shift down the CBM of lead mixed-halide perovskite decreasing the band gap of $CsMX_3$. This is in good agreement with the intermediate states that $CsPb_{0.9}Sn_{0.1}IBr_2$ film has longer wavelength than $CsPbIBr_2$. However, the initial PL for $CsPb_{0.9}Sn_{0.1}IBr_2$ (576 nm) is slightly blueshifted than $CsPbIBr_2$ (584 nm), which is contradictory. This should be due to the exciton binding energy of $CsPbIBr_2$ is much higher than that of Sn^{2+}-doped perovskite (Li et al., 2018a; Long et al., 2019; Galkowski et al., 2019), which can also be verified by the comparisons from the absorption spectra of these two samples (Figure S2). In addition, the detailed structure and band gap of the intermediate state is still unclear. It is possible that the ratio between the halide

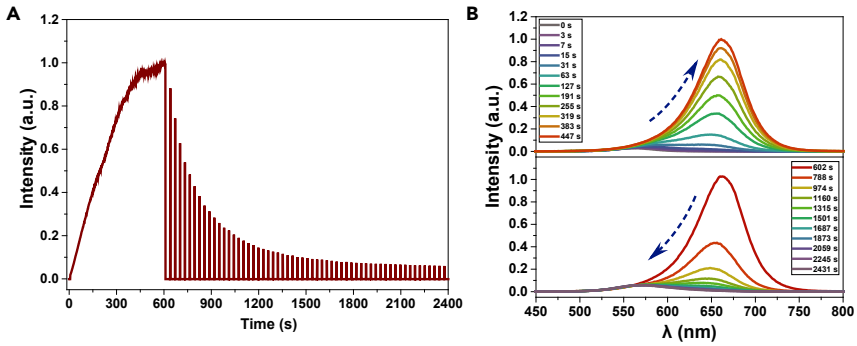

Figure 4. Reversibility of the PL Variations in $CsPb_{0.9}Sn_{0.1}IBr_2$ Films

(A) PL intensity variations of $CsPb_{0.9}Sn_{0.1}IBr_2$ films. The first 600 s was measured under continuous irradiation, whereas the following 1,800 s was the PL intensity measured for 1 s and then kept in dark for the duration of 30 s.

(B) The corresponding PL wavelength variations of the two stages. The excitation wavelength was 450 nm and the power density was 5 W/cm^2. The measurements were taken under N_2 atmosphere.

elements could be different for $CsPbIBr_2$ and $CsPb_{0.9}Sn_{0.1}IBr_2$, which significantly affects the band gap of the intermediate state. Therefore, the redshifted PL spectrum from $CsPb_{0.9}Sn_{0.1}IBr_2$ intermediate state compared with that from $CsPbIBr_2$ intermediated state can be due to decrease of band gap after Sn^{2+} doping and/or different I/Br ratio of the intermediate state. Characterization of the intermediate state is still undergoing in our group by employing more *in situ* measurements.

Reversibility of the PL Properties of $CsPb_{0.9}Sn_{0.1}IBr_2$ Films

As can be seen from the above discussion, the stable PL emission from $CsPb_{0.9}Sn_{0.1}IBr_2$ films was achieved by light soaking. To confirm that the emission is from a state of $CsPb_{0.9}Sn_{0.1}IBr_2$ material stabilized by Sn^{2+} doping, we have to exclude any light-induced irreversible variation that may permanently change the properties of the films. Thus, we checked the reversibility of this light soaking process, as shown in Figure 4. Under continuous light excitation, the PL intensity kept increasing and the spectrum redshifted to ~650 nm, similar to the results shown in Figure 2A. When the excitation light was turned off, the PL intensity decreased and the spectrum blueshifted back to the initial state. To investigate the recovery process without significantly affecting it, we detected the PL spectra and PL intensity for 1 s and then kept in dark with a time interval of 30 s, as shown in Figure 4. Moreover, if we keep the film in dark for ~5 min and then switch on the excitation light again, the material can recover to the initial state and the PL enhancement and spectral shift process can be well repeated, as shown in Figure S3. Therefore, we can conclude that the intermediate state phase in the Sn^{2+}-doped lead mixed-halide perovskites can only be stabilized under light irradiation.

Spectral Variation after the Oxidization of Sn^{2+} Ions

Photo-induced phase segregation behavior has been widely observed in organic-inorganic hybrid lead mixed-halide perovskites (Hoke et al., 2015). All-inorganic Cs-based mixed-halide perovskites that exhibit brilliant stability against moisture also have the same problem (Li et al., 2017). The phase segregation process was proposed to be originated from the ion migration affected by lattice strain (Hoke et al., 2015). The expansion of lattice strain could result from the incompatible sizes of halide atoms, which will increase the Helmholtz free energy of $CsPbI_xBr_{3-x}$ (Beal et al., 2016; Yin et al., 2014). Under illumination, the interatomic separations along distinct directions (e.g., Pb-I and Pb-Br) will take place to minimize the internal strain (Bischak et al., 2017; Brivio et al., 2016). However, the partial substitution of Pb^{2+} by Sn^{2+} in $CsPbI_xBr_{1-x}$ will lead to the shrinkage of perovskite lattice, indicating that the reduction of lattice strain in $CsPb_{0.9}Sn_{0.1}I_xBr_{3-x}$ should also correlate with the decrease of Helmholtz free energy (Li et al., 2018b). Therefore, with the substitution of Sn^{2+}, the photo-excitation can drive $CsPb_{0.9}Sn_{0.1}IBr_2$ to form a stable intermediate phase state ($CsPb_{0.9}Sn_{0.1}I_xBr_{3-x}$), which possesses the minimum lattice strain and will not continue to segregate into two different phases. Besides the light-induced segregation, the photo-stability of $CsPb_{0.9}Sn_{0.1}IBr_2$ was also significantly improved, which can also be explained by the reduction of the lattice strain.

To further verify the effect of Sn^{2+} doping, we tried to oxidize the Sn^{2+} ions to Sn^{4+} by two different ways to check the effect on phase segregation. As well known, Sn^{2+} cations can be easily oxidized to Sn^{4+} under

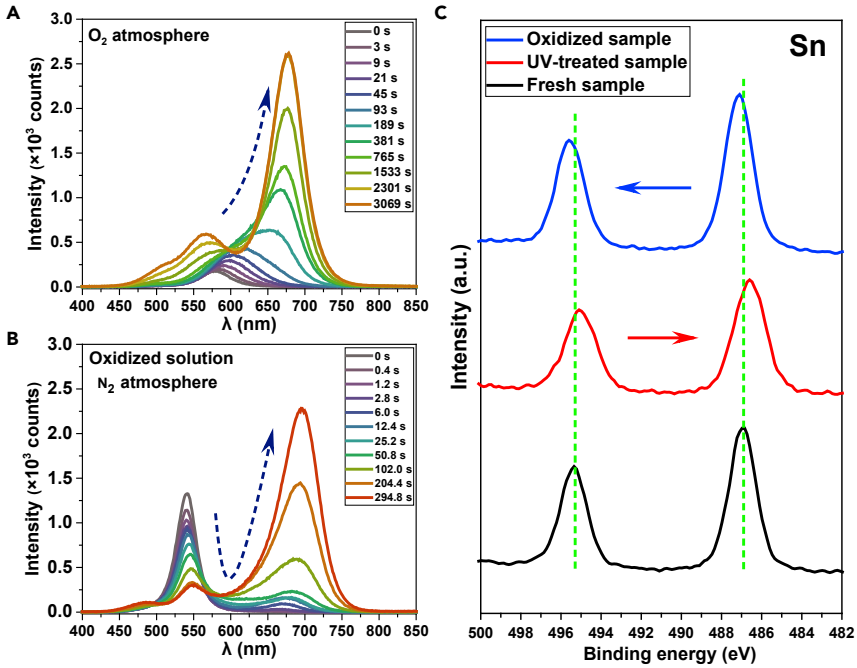

Figure 5. PL Variations of $CsPb_{0.9}Sn_{0.1}IBr_2$ Films Treated by Different Conditions

(A) PL emissions of $CsPb_{0.9}Sn_{0.1}IBr_2$ film exposed under an oxygen atmosphere.

(B) PL emissions of $CsPb_{0.9}Sn_{0.1}IBr_2$ film fabricated by using the precursor solution that was pre-oxidized before spin-casting. And the PL measurements in (B) were taken under nitrogen atmosphere. The samples in both (A) and (B) were excited by a 450-nm-wavelength laser with a power density of 5 W/cm^2.

(C) XPS analysis of Sn element in $CsPb_{0.9}Sn_{0.1}IBr_2$ films, and the three samples were fresh sample, UV-treated sample, and oxidized sample, respectively.

ambient environment (Jung et al., 2016; Kwoka et al., 2005). To confirm whether Sn^{2+} played a significant role in stabilizing the intermediate phase of $CsPb_{0.9}Sn_{0.1}IBr_2$, we introduced an oxygen flow surrounding the $CsPb_{0.9}Sn_{0.1}IBr_2$ film and simultaneously detected the PL variations. In Figure 5A, the PL emission started from a single peak and slowly transformed into two peaks under continuous irradiation in an oxygen atmosphere, which showed the same tendency as the $CsPbIBr_2$ film exposed under oxygen atmosphere (see Figure S4). Although the oxygen atmospheres will complicate the PL emissions of the perovskite, they mainly involve with the PL intensity rather than with the PL spectra, which can also be verified from the PL variation of $CsPbIBr_2$ film measured under oxygen atmosphere. The PL variation only differs from that under nitrogen atmosphere in the PL intensity, because the defects in $CsPbIBr_2$ were always susceptible to different atmosphere (Fang et al., 2016; Galisteo-López et al., 2015; Tian et al., 2015). The small peak near 500 nm could be derived from the PL emissions of PbI_2 and $PbBr_2$ formed by the degradation of perovskite crystals. As discussed before, by comparing the PL emissions of $CsPbIBr_2$ and $CsPbSnIBr_2$ under N_2 atmospheres we can conclude the effects of the doped Sn^{2+} ions. Then, according to that the photoinduced phase segregation of $CsPb_{0.9}Sn_{0.1}IBr_2$ perovskite only happens in O_2 atmosphere, which should be due to the destructive effects of Sn^{2+}, the inhibition effects of Sn^{2+} doping can be further confirmed. In addition, we took another method to directly oxidize the Sn^{2+} ions. Before the perovskite film was fabricated, the precursor solution was pre-oxidized under ambient environment. Figure 5B showed the PL emissions of the $CsPb_{0.9}Sn_{0.1}IBr_2$ film prepared by spin-casting the pre-oxidized precursor solution. The photoinduced phase segregation processes of this perovskite film under nitrogen atmosphere can be directly observed, which is similar to that in Figure 2D. Subsequently, we further changed the atmosphere to oxygen (see Figure S5) and verified that the PL variation of $CsPb_{0.9}Sn_{0.1}IBr_2$ film prepared by pre-oxidized solution showed no difference with that of $CsPbIBr_2$ film after the oxidization of Sn^{2+}. To confirm the valence state change from Sn^{2+} to Sn^{4+} in $CsPb_{0.9}Sn_{0.1}IBr_2$, we also performed XPS analysis for comparison. Three different samples were measured by XPS: (1) film fabricated from fresh precursor solution (named as "fresh sample"); (2) film fabricated from fresh precursor solution and then treated under UV light in oxygen atmosphere for 30 min (named as "UV-treated sample"); (3) film fabricated from pre-oxidized precursor solution

(named as "oxidized sample"). The binding energies of C1s bands were all recalibrated to 284.6 eV (Briggs et al., 1981). As shown in Figure 5C, compared with the fresh sample, the binding energies of Sn species in the UV-treated sample moved to lower levels, which shall be ascribed to the formation of SnO_2, in which the electronegativity of oxygen is lower than that of halide, thus leading to the decrease of binding energy of Sn^{4+}. As showed in Figure S6, the increase of oxygen contents in the UV-treated sample was also detected by XPS, further confirming the formation of SnO_2 on the surface of perovskite films. In contrast, the binding energies of Sn species in the oxidized sample moved to higher levels, corresponding to the valence state change from Sn^{2+} to Sn^{4+}, which indicated the presence of Sn^{4+} in the oxidized sample. The oxidization from Sn^{2+} to Sn^{4+} would destroy the octahedron structures of mixed-halide perovskites (Leijtens et al., 2017; Qiu et al., 2017) and thus result in the increase of lattice strain; consequently, the light-induced phase segregation reoccurred. As a whole, the above results proved the effective inhibition functions of Sn^{2+} dopants in $CsPb_{0.9}Sn_{0.1}IBr_2$.

Destructive Effects of Moisture on Sn^{2+} Based Mixed-Halide Perovskite Films

The study presented above has successfully assessed the impact of doped Sn^{2+} ions in $CsPb_{0.9}Sn_{0.1}IBr_2$. However, it also reflected the shortcoming of mixed-halide perovskites that is easily susceptible to the ambient atmosphere. Although $CsPb_{0.9}Sn_{0.1}IBr_2$ exhibits brilliant stability against phase segregation and photo-degradation under nitrogen atmosphere, it is still labile when getting in touch with oxygen and moisture. Figure S7 shows the time-dependent PL traces and variations of PL spectra when exposed in ambient atmosphere with a relative humidity of 40%. Both photo-induced phase segregation and photo-degradation gradually appeared after 10 min, which should be attributed to the synergistic influence of oxygen and H_2O in air. We also checked the PL variation in oxygen atmosphere mixed with H_2O vapor, as shown in Figure S8. The photo-induced segregation even cannot catch up with photo-degradation processes, and finally, the whole perovskite phase turned into lead halide phase (Baibarac et al., 2015). For the fact that $CsPbI_3$ perovskite was thermodynamically unfavorable under room temperature and very prone to exhibit phase transition in ambient atmosphere (Eperon et al., 2015; Kulbak et al., 2015; Luo et al., 2016; Yunakova et al., 2012), the photo-induced phase segregation was almost masked owing to the fast disappearance of iodine-rich phase in the mixed atmosphere of oxygen and H_2O. These results also explain why the long-term stability of $CsPb_xSn_{1-x}IBr_2$ perovskite solar cells can be well maintained when protected by encapsulation (Li et al., 2018b; Liang et al., 2017), which can help to isolate the perovskite materials from the oxygen and humidity in air.

Improved Tolerance to Ambient Atmosphere by Doping Mn^{2+} in B Site

As discussed above, the Sn^{2+} is easy to be oxidized into Sn^{4+} or SnO_2 after interacting with oxygen and moisture (Ke et al., 2017; Liao et al., 2016) leading to the light-induced phase segregation behaviors. To solve this problem and improve the tolerance of mixed-halide perovskite to oxygen and moisture, we tried to use Mn^{2+} instead of Sn^{2+} because Mn^{2+} is very difficult to be directly oxidized into MnO_2 by oxygen (Diem and Stumm, 1984; Feng et al., 2004) and can be effectively introduced into the lattice of $CsPbX_3$ perovskites (Liang et al., 2018). We prepared the $CsPb_{0.99}Mn_{0.01}IBr_2$ films by one-step method and further characterized the X-ray diffraction pattern (Figure S9). Also, the HR-TEM images were taken and shown in Figure S10. From the comparisons among undoped, Sn^{2+}-doped, and Mn^{2+}-doped samples, we can observe that, as the ionic radius of B-site ions decreases, the diffraction angles are increased and the lattice distances are reduced. And according to Bragg's law we can also conclude that the lattice distance obtained in Figure S10 corresponds to (200) planes of cubic Pm-3m phase (PDF#84-0464). Thus the results obtained from XRD and HR-TEM confirm that the Sn^{2+} and Mn^{2+} ions are successfully doped into the perovskite crystals leading to the lattice shrinkage that can effectively help to release the lattice strain. Then we measured the PL spectra under ambient atmosphere to compare with $CsPb_{0.9}Sn_{0.1}IBr_2$ films. As shown in Figure 6A, the PL behavior of $CsPb_{0.99}Mn_{0.01}IBr_2$ is very similar to that of $CsPb_{0.9}Sn_{0.1}IBr_2$ shown in Figure 2, which was measured in N_2 atmosphere. The initial PL spectrum of $CsPb_{0.99}Mn_{0.01}IBr_2$ film also showed a single peak (the inset of Figure 6A), and the PL intensity significantly increased for more than 100 times under light irradiation with the maximal position shifted to 676 nm in 10 min as shown in Figure 6B. The most important difference between these two samples was the atmosphere effect. As shown in Figure S7 and discussed in previous sections, clear phase segregation of $CsPb_{0.9}Sn_{0.1}IBr_2$ can be observed owing to the oxidization of Sn^{2+}. However, for $CsPb_{0.99}Mn_{0.01}IBr_2$, no phase segregation was observed after 20 min light irradiation in air verifying the improved tolerance to oxygen and moisture with doped Mn^{2+} in the B site of the perovskite. Therefore, B-site doping with Mn^{2+} ions should be a promising way to inhibit the light-induced phase segregation of mixed-halide perovskite materials and can simultaneously improve

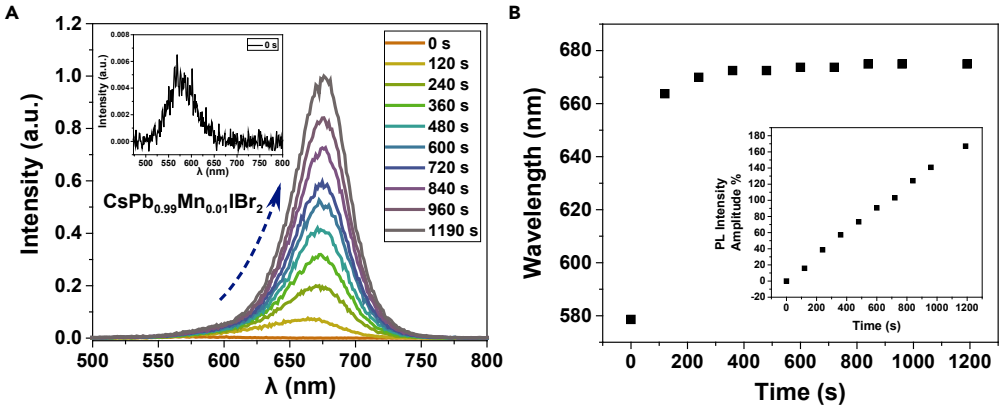

Figure 6. Real-Time PL Monitoring of $CsPb_{0.99}Mn_{0.01}IBr_2$ Films

(A) PL variations of $CsPb_{0.99}Mn_{0.01}IBr_2$ film under continuous irradiation.The inset in (A) shows the initial PL spectrum. (B) PL peak wavelength in (A) varied as irradiation time. The inset in (B) shows the variation of the PL intensity amplitude under continuous irradiation. The amplitude is calculated by $(I - I_0)/I_0$, where I_0 indicates the initial PL intensity and I indicates the varied PL intensity. The sample was excited by a 450-nm laser with a power density of 5 W/cm^2, and the PL measurements were taken under ambient atmosphere.

the stability in ambient atmosphere. In addition, other divalent cations including Zn^{2+}, Cd^{2+}, and alkaline-earth metals are reported to have been successfully incorporated into $CsPbX_3$ nanocrystals (Cai et al., 2018; Chen et al., 2019; van der Stam et al., 2017). We believe that the doping of these ions will also affect the stability of the materials. However, it is difficult to predict whether they will have positive or negative effect before we perform systematic investigation.

Conclusion

In summary, we investigated the light-induced phase segregation processes in Cs-based mixed-halide perovskites by monitoring the real-time PL spectra. We found that the partial substitution of Pb^{2+} by Sn^{2+} in cesium-based lead mixed-halide perovskites can significantly inhibit the photo-induced phase segregation. As a typical Sn^{2+}-doped mixed-halide perovskite, $CsPb_{0.9}Sn_{0.1}IBr_2$ exhibits brilliant photo-stability in inert gas atmosphere from two aspects: (1) the stable mixed-halide perovskite phase without phase segregation; 2) the high tolerance to high excitation power with nearly no photo-degradation after long-time light irradiation. The photo-stability brought by Sn^{2+} doping could be originated from the release of lattice strain in the crystal structure of Sn^{2+}-doped perovskite film. However, such stability can be easily destroyed by the oxidization of Sn^{2+} into Sn^{4+} when exposed to oxygen atmosphere. Control experiments and XPS analysis proved that the oxidization of Sn^{2+} could lead to phase separation confirming that B-site doping was an effective method to inhibit the light-induced phase separation. To improve the stability of ions in B sites, we replaced dopant ions Sn^{2+} by Mn^{2+} and successfully improved the tolerance against ambient atmosphere. We believe our findings provide an efficient way to prevent the phase separation process of mixed-halide perovskites and have significant values for the development of stable and efficient all-inorganic perovskite photovoltaic and light-emitting devices.

Limitations of the Study

In this work, we found that B-site doping by Sn^{2+} or Mn^{2+} can effectively improve the photo-stability and inhibit the light-induced phase segregation of the mixed-halide perovskite. However, according to our results, it takes time to reach the stable phase depending on the light intensity, which could affect the application of these materials. Further optimization of the stable phase is needed.

Resource Availability

Lead Contact

Further information and requests for resources and reagents should be directed to and will be fulfilled by the Lead Contact, Prof. Yuxi Tian (tyx@nju.edu.cn).

Materials Availability

The study did not generate new unique reagents.

Data and Code Availability

The published article includes all datasets/code generated or analyzed during this study. Supplemental Informationtyx@nju.edu.cn

METHODS

All methods can be found in the accompanying Transparent Methods supplemental file.

SUPPLEMENTAL INFORMATION

Supplemental Information can be found online at https://doi.org/10.1016/j.isci.2020.101415.

ACKNOWLDEGEMENTS

This work is supported by National Natural Science Foundation of China (NSFC No. 21673114, No.62011530133, No. 21872069, No. 51761135104, No. 21573108), National Key R&D Program of China (2017YFA0208200, 2016YFB0700600, 2015CB659300), and the Natural Science Foundation of Jiangsu Province (No. BK20180008).

AUTHOR CONTRIBUTIONS

D.H. carried out the SEM, UV-absorption, and XRD characterizations. P.Z. and C.Z. prepared the stock solutions for film fabrication. Y.X. and Z.W. offered assistance for the TEM characterizations and analyses. D. H. and Y. D. carried out the PL measurements and data analysis. D.H. and Y.T. wrote the manuscript. The project was under supervision of Y.T. and Z.J., and all authors were involved in discussions and the writing process.

DECLARATION OF INTERESTS

No competing interests are declared.

Received: March 11, 2020
Revised: June 26, 2020
Accepted: July 27, 2020
Published: August 21, 2020

REFERENCES

Baibarac, M., Smaranda, I., Scocioreanu, M., Mitran, R.A., Enculescu, M., Galatanu, M., and Baltog, I. (2015). Exciton-phonon interaction in PbI_2 revealed by Raman and photoluminescence studies using excitation light overlapping the fundamental absorption edge. Mater. Res. Bull. *70*, 762–772.

Beal, R.E., Slotcavage, D.J., Leijtens, T., Bowring, A.R., Belisle, R.A., Nguyen, W.H., Burkhard, G.F., Hoke, E.T., and McGehee, M.D. (2016). Cesium lead halide perovskites with improved stability for Tandem solar cells. J. Phys. Chem. Lett. *7*, 746–751.

Bi, C., Wang, Q., Shao, Y., Yuan, Y., Xiao, Z., and Huang, J. (2015). Non-wetting surface-driven high-aspect-ratio crystalline grain growth for efficient hybrid perovskite solar cells. Nat. Commun. *6*, 7747.

Bischak, C.G., Hetherington, C.L., Wu, H., Aloni, S., Ogletree, D.F., Limmer, D.T., and Ginsberg, N.S. (2017). Origin of reversible photoinduced phase separation in hybrid perovskites. Nano Lett. *17*, 1028–1033.

Brandt, R.E., Stevanović, V., Ginley, D.S., and Buonassisi, T. (2015). Identifying defect-tolerant semiconductors with high minority-carrier lifetimes: beyond hybrid lead halide perovskites. MRS Commun. *5*, 265–275.

Briggs, D., Wanger, C.D., Riggs, W.M., Davis, L.E., Moulder, J.F., and Muilenberg, G.E. (1981). Handbook of X-Ray Photoelectron Spectroscopy (Perkin-Elmer Corp)).

Brivio, F., Caetano, C., and Walsh, A. (2016). Thermodynamic origin of photoinstability in the $CH_3NH_3Pb(I_{1-x}Br_x)_3$ hybrid halide perovskite alloy. J. Phys. Chem. Lett. *7*, 1083–1087.

Cai, T., Yang, H., Hills-Kimball, K., Song, J.-P., Zhu, H., Hofman, E., Zheng, W., Rubenstein, B.M., and Chen, O. (2018). Synthesis of all-inorganic Cd-doped $CsPbCl_3$ perovskite nanocrystals with dual-wavelength emission. J. Phys. Chem. Lett. *9*, 7079–7084.

Cao, Y., Wang, N., Tian, H., Guo, J., Wei, Y., Chen, H., Miao, Y., Zou, W., Pan, K., He, Y., et al. (2018). Perovskite light-emitting diodes based on spontaneously formed submicrometre-scale structures. Nature *562*, 249–253.

Chang, X., Li, W., Zhu, L., Liu, H., Geng, H., Xiang, S., Liu, J., and Chen, H. (2016). Carbon-based $CsPbBr_3$ perovskite solar cells: all-ambient processes and high thermal stability. ACS Appl. Mater. Interfaces *8*, 33649–33655.

Chen, J.-K., Ma, J.-P., Guo, S.-Q., Chen, Y.-M., Zhao, Q., Zhang, B.-B., Li, Z.-Y., Zhou, Y., Hou, J., Kuroiwa, Y., et al. (2019). High-efficiency violet-emitting all-inorganic perovskite nanocrystals enabled by alkaline-earth metal passivation. Chem. Mater. *31*, 3974–3983.

Diem, D., and Stumm, W. (1984). Is dissolved Mn^{2+} being oxidized by O_2 in absence of Mn-bacteria or surface catalysts? Geochim. Cosmochim. Acta *48*, 1571–1573.

Duan, J., Zhao, Y., He, B., and Tang, Q. (2018). High-purity inorganic perovskite films for solar cells with 9.72 % efficiency. Angew. Chem. Int. Ed. *57*, 3787–3791.

Eperon, G.E., Paternò, G.M., Sutton, R.J., Zampetti, A., Haghighirad, A.A., Cacialli, F., and Snaith, H.J. (2015). Inorganic caesium lead iodide perovskite solar cells. J. Mater. Chem. A *3*, 19688–19695.

Fang, H.-H., Adjokatse, S., Wei, H., Yang, J., Blake, G.R., Huang, J., Even, J., and Loi, M.A. (2016). Ultrahigh sensitivity of methylammonium lead tribromide perovskite single crystals to environmental gases. Sci. Adv. *2*, e1600534.

Feng, X.H., Liu, F., Tan, W.F., and Liu, X.W. (2004). Synthesis of Birnessite from the oxidation of Mn^{2+} by O_2 in alkali medium: effects of synthesis conditions. Clays Clay Miner. *52*, 240–250.

Galisteo-López, J.F., Anaya, M., Calvo, M.E., and Míguez, H. (2015). Environmental effects on the photophysics of organic–inorganic halide perovskites. J. Phys. Chem. Lett. *6*, 2200–2205.

Galkowski, K., Surrente, A., Baranowski, M., Zhao, B., Yang, Z., Sadhanala, A., Mackowski, S., Stranks, S.D., and Plochocka, P. (2019). Excitonic properties of low-band-gap Lead–Tin halide perovskites. ACS Energy Lett *4*, 615–621.

Green, M.A., Ho-Baillie, A., and Snaith, H.J. (2014). The emergence of perovskite solar cells. Nat. Photon. *8*, 506–514.

Han, Y., Meyer, S., Dkhissi, Y., Weber, K., Pringle, J.M., Bach, U., Spiccia, L., and Cheng, Y.-B. (2015). Degradation observations of encapsulated planar $CH_3NH_3PbI_3$ perovskite solar cells at high temperatures and humidity. J. Mater. Chem. A *3*, 8139–8147.

Hao, F., Stoumpos, C.C., Chang, R.P.H., and Kanatzidis, M.G. (2014). Anomalous band gap behavior in mixed Sn and Pb perovskites enables broadening of absorption spectrum in solar cells. J. Am. Chem. Soc. *136*, 8094–8099.

Hoke, E.T., Slotcavage, D.J., Dohner, E.R., Bowring, A.R., Karunadasa, H.I., and McGehee, M.D. (2015). Reversible photo-induced trap formation in mixed-halide hybrid perovskites for photovoltaics. Chem. Sci. *6*, 613–617.

Jiang, J., Jin, Z., Gao, F., Sun, J., Wang, Q., and Liu, S.F. (2018). $CsPbCl_3$ -driven low-trap-density perovskite grain growth for >20% solar cell efficiency. Adv. Sci. *5*, 1800474.

Jiang, Q., Zhang, L., Wang, H., Yang, X., Meng, J., Liu, H., Yin, Z., Wu, J., Zhang, X., and You, J. (2017). Enhanced electron extraction using SnO_2 for high-efficiency planar-structure $HC(NH_2)_2PbI_3$-based perovskite solar cells. Nat. Energy *2*, 16177.

Jung, M.-C., Raga, S.R., and Qi, Y. (2016). Properties and solar cell applications of Pb-free perovskite films formed by vapor deposition. RSC Adv. *6*, 2819–2825.

Ke, W., Stoumpos, C.C., Spanopoulos, I., Mao, L., Chen, M., Wasielewski, M.R., and Kanatzidis, M.G. (2017). Efficient lead-free solar cells based on hollow {en}$MASnI_3$ perovskites. J. Am. Chem. Soc. *139*, 14800–14806.

Klug, M.T., Osherov, A., Haghighirad, A.A., Stranks, S.D., Brown, P.R., Bai, S., Wang, J.T.-W., Dang, X., Bulović, V., Snaith, H.J., and Belcher, A.M. (2017). Tailoring metal halide perovskites through metal substitution: influence on photovoltaic and material properties. Energy Environ. Sci. *10*, 236–246.

Kulbak, M., Cahen, D., and Hodes, G. (2015). How important is the organic part of lead halide perovskite photovoltaic cells? Efficient $CsPbBr_3$ cells. J. Phys. Chem. Lett. *6*, 2452–2456.

Kwoka, M., Ottaviano, L., Passacantando, M., Santucci, S., Czempik, G., and Szuber, J. (2005). XPS study of the surface chemistry of L-CVD SnO_2 thin films after oxidation. Thin Solid Films *490*, 36–42.

Leijtens, T., Eperon, G.E., Noel, N.K., Habisreutinger, S.N., Petrozza, A., and Snaith, H.J. (2015). Stability of metal halide perovskite solar cells. Adv. Energy Mater. *5*, 1500963.

Leijtens, T., Prasanna, R., Gold-Parker, A., Toney, M.F., and McGehee, M.D. (2017). Mechanism of Tin oxidation and stabilization by lead substitution in Tin halide perovskites. ACS Energy Lett *2*, 2159–2165.

Li, B., Long, R., Xia, Y., and Mi, Q. (2018a). All-inorganic perovskite $CsSnBr_3$ as a thermally stable, free-carrier semiconductor. Angew. Chem. Int. Ed. *57*, 13154–13158.

Li, N., Zhu, Z., Li, J., Jen, A.K.-Y., and Wang, L. (2018b). Inorganic $CsPb_{1-x}Sn_xIBr_2$ for efficient wide-bandgap perovskite solar cells. Adv. Energy Mater. *8*, 1800525.

Li, W., Rothmann, M.U., Liu, A., Wang, Z., Zhang, Y., Pascoe, A.R., Lu, J., Jiang, L., Chen, Y., Huang, F., et al. (2017). Phase segregation enhanced ion movement in efficient inorganic $CsPbIBr_2$ solar cells. Adv. Energy Mater. *7*, 1700946.

Liang, J., Liu, Z., Qiu, L., Hawash, Z., Meng, L., Wu, Z., Jiang, Y., Ono, L.K., and Qi, Y. (2018). Enhancing optical, electronic, crystalline, and morphological properties of cesium lead halide by Mn substitution for high-stability all-inorganic perovskite solar cells with carbon electrodes. Adv. Energy Mater. *8*, 1800504.

Liang, J., Wang, C., Wang, Y., Xu, Z., Lu, Z., Ma, Y., Zhu, H., Hu, Y., Xiao, C., Yi, X., et al. (2016). All-inorganic perovskite solar cells. J. Am. Chem. Soc. *138*, 15829–15832.

Liang, J., Zhao, P., Wang, C., Wang, Y., Hu, Y., Zhu, G., Ma, L., Liu, J., and Jin, Z. (2017). $CsPb_{0.9}Sn_{0.1}IBr_2$ based all-inorganic perovskite solar cells with exceptional efficiency and stability. J. Am. Chem. Soc. *139*, 14009–14012.

Liao, W., Zhao, D., Yu, Y., Grice, C.R., Wang, C., Cimaroli, A.J., Schulz, P., Meng, W., Zhu, K., Xiong, R.-G., and Yan, Y. (2016). Lead-free inverted planar Formamidinium Tin Triiodide perovskite solar cells achieving power conversion efficiencies up to 6.22%. Adv. Mater. *28*, 9333–9340.

Lin, K., Xing, J., Quan, L.N., de Arquer, F.P.G., Gong, X., Lu, J., Xie, L., Zhao, W., Zhang, D., Yan, C., et al. (2018). Perovskite light-emitting diodes with external quantum efficiency exceeding 20 per cent. Nature *562*, 245–248.

Long, H., Peng, X., Lin, K., Xie, L., Lu, J., Zhang, B., Ying, L., and Wei, Z. (2019). Acoustic phonon–exciton interaction by extremely strong exciton confinement and large phonon energy in $CsPbBr_3$ perovskite. Appl. Phys. Express *12*, 052003.

Luo, P., Xia, W., Zhou, S., Sun, L., Cheng, J., Xu, C., and Lu, Y. (2016). Solvent engineering for ambient-air-processed, phase-stable $CsPbI_3$ in perovskite solar cells. J. Phys. Chem. Lett. *7*, 3603–3608.

Matsumoto, F., Vorpahl, S.M., Banks, J.Q., Sengupta, E., and Ginger, D.S. (2015). Photodecomposition and morphology evolution of organometal halide perovskite solar cells. J. Phys. Chem. C *119*, 20810–20816.

Mosconi, E., Azpiroz, J.M., and De Angelis, F. (2015). Ab Initio molecular dynamics simulations of methylammonium lead iodide perovskite degradation by water. Chem. Mater. *27*, 4885–4892.

Niezgoda, J.S., Foley, B.J., Chen, A.Z., and Choi, J.J. (2017). Improved charge collection in highly efficient $CsPbBrI_2$ solar cells with light-induced dealloying. ACS Energy Lett *2*, 1043–1049.

Noh, J.H., Im, S.H., Heo, J.H., Mandal, T.N., and Seok, S.I. (2013). Chemical management for colorful, efficient, and stable inorganic–organic hybrid nanostructured solar cells. Nano Lett. *13*, 1764–1769.

NREL. (2020). Best Research-Cell Efficiency Chart. https://www.nrel.gov/pv/cell-effciency.html.

Ono, L.K., Qi, Y., and Liu, S.F. (2018). Progress toward stable lead halide perovskite solar cells. Joule *2*, 1961–1990.

Qiu, X., Cao, B., Yuan, S., Chen, X., Qiu, Z., Jiang, Y., Ye, Q., Wang, H., Zeng, H., Liu, J., and Kanatzidis, M.G. (2017). From unstable $CsSnI_3$ to air-stable Cs_2SnI_6: a lead-free perovskite solar cell light absorber with bandgap of 1.48 eV and high absorption coefficient. Sol. Energy Mater. Sol. Cells *159*, 227–234.

Slotcavage, D.J., Karunadasa, H.I., and McGehee, M.D. (2016). Light-induced phase segregation in halide-perovskite absorbers. ACS Energy Lett *1*, 1199–1205.

Snaith, H.J. (2013). Perovskites: the emergence of a new era for low-cost, high-efficiency solar cells. J. Phys. Chem. Lett. *4*, 3623–3630.

Stranks, S.D. (2017). Nonradiative losses in metal halide perovskites. ACS Energy Lett *2*, 1515–1525.

Tan, Z., Moghaddam, R.S., Lai, M.L., Docampo, P., Higler, R., Deschler, F., Price, M., Sadhanala, A., Pazos, L.M., Credgington, D., et al. (2014). Bright light-emitting diodes based on organometal halide perovskite. Nat. Nanotechnol. *9*, 687–692.

Tian, Y., Peter, M., Unger, E., Abdellah, M., Zheng, K., Pullerits, T., Yartsev, A., Sundström, V., and Scheblykin, I.G. (2015). Mechanistic insights into perovskite photoluminescence enhancement: light curing with oxygen can boost yield thousandfold. Phys. Chem. Chem. Phys. *17*, 24978–24987.

van der Stam, W., Geuchies, J.J., Altantzis, T., van den Bos, K.H.W., Meeldijk, J.D., Van Aert, S., Bals, S., Vanmaekelbergh, D., and de Mello Donega, C. (2017). Highly emissive divalent-ion-doped colloidal $CsPb_{1-x}M_xBr_3$ perovskite nanocrystals

through cation exchange. J. Am. Chem. Soc. *139*, 4087–4097.

Wang, K., Jin, Z., Liang, L., Bian, H., Bai, D., Wang, H., Zhang, J., Wang, Q., and Liu, S. (2018). All-inorganic cesium lead iodide perovskite solar cells with stabilized efficiency beyond 15%. Nat. Commun. *9*, 4544.

Wu, Y., Yang, X., Chen, W., Yue, Y., Cai, M., Xie, F., Bi, E., Islam, A., and Han, L. (2016). Perovskite solar cells with 18.21% efficiency and area over 1 cm^2 fabricated by heterojunction engineering. Nat. Energy *1*, 16148.

Yang, X., Yan, X., Wang, W., Zhu, X., Li, H., Ma, W., and Sheng, C. (2016). Light induced metastable modification of optical properties in $CH_3NH_3PbI_{3-x}Br_x$ perovskite films: two-step mechanism. Org. Electron. *34*, 79–83.

Yin, W.-J., Yan, Y., and Wei, S.-H. (2014). Anomalous alloy properties in mixed halide perovskites. J. Phys. Chem. Lett. *5*, 3625–3631.

Yunakova, O.N., Miloslavskii, V.K., and Kovalenko, E.N. (2012). Exciton absorption spectrum of thin $CsPbI_3$ and Cs_4PbI_6 films. Opt. Spectrosc. *112*, 91–96.

Zhang, H., Fu, X., Tang, Y., Wang, H., Zhang, C., Yu, W.W., Wang, X., Zhang, Y., and Xiao, M. (2019). Phase segregation due to ion migration in all-inorganic mixed-halide perovskite nanocrystals. Nat. Commun. *10*, 1088.

iScience, Volume *23*

Supplemental Information

Inhibition of Phase Segregation in Cesium Lead Mixed-Halide Perovskites by B-Site Doping

Daocheng Hong, Peiyang Zhao, Yu Du, Cheng Zhao, Yuren Xia, Zhihong Wei, Zhong Jin, and Yuxi Tian

Figures:

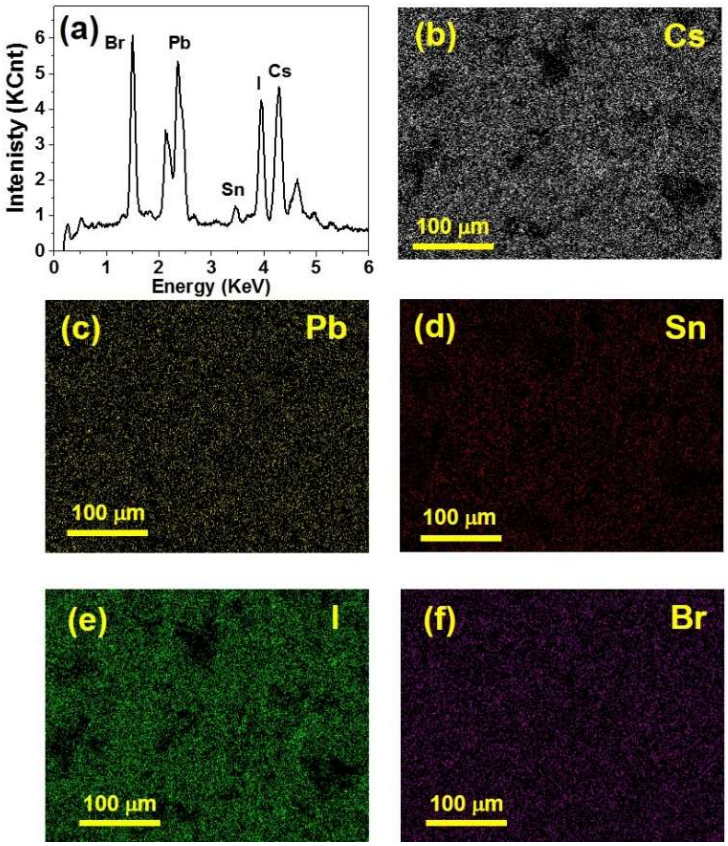

Figure S1. (a) EDX analysis of $CsPb_{0.9}Sn_{0.1}IBr_2$ film. (b-f) 2D spatial elemental mappings of Cs, Pb, Sn, Br and I elements, respectively. Related to Figure 1.

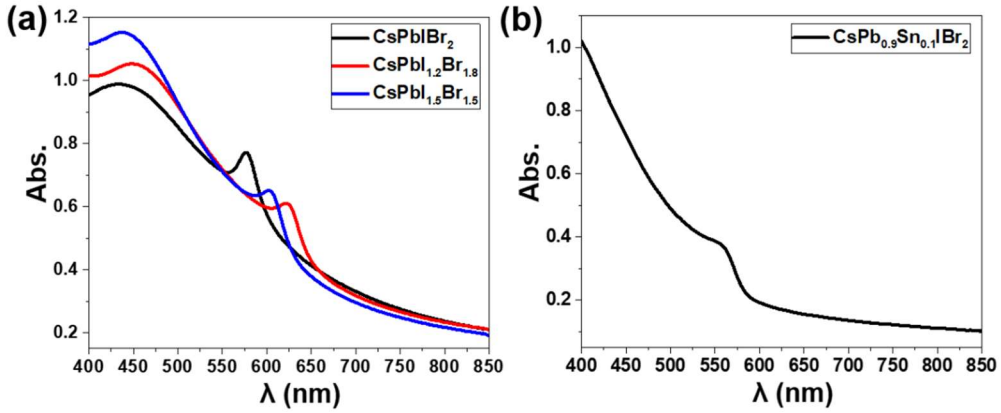

Figure S2. (a) The absorption spectra of lead mixed-halide perovskite with different I/Br ratios ($CsPbIBr_2$, $CsPbI_{1.2}Br_{1.8}$, $CsPbI_{1.5}Br_{1.5}$). (b) The absorption spectra of $CsPb_{0.9}Sn_{0.1}IBr_2$. Related to Figure 2 and Figure 3.

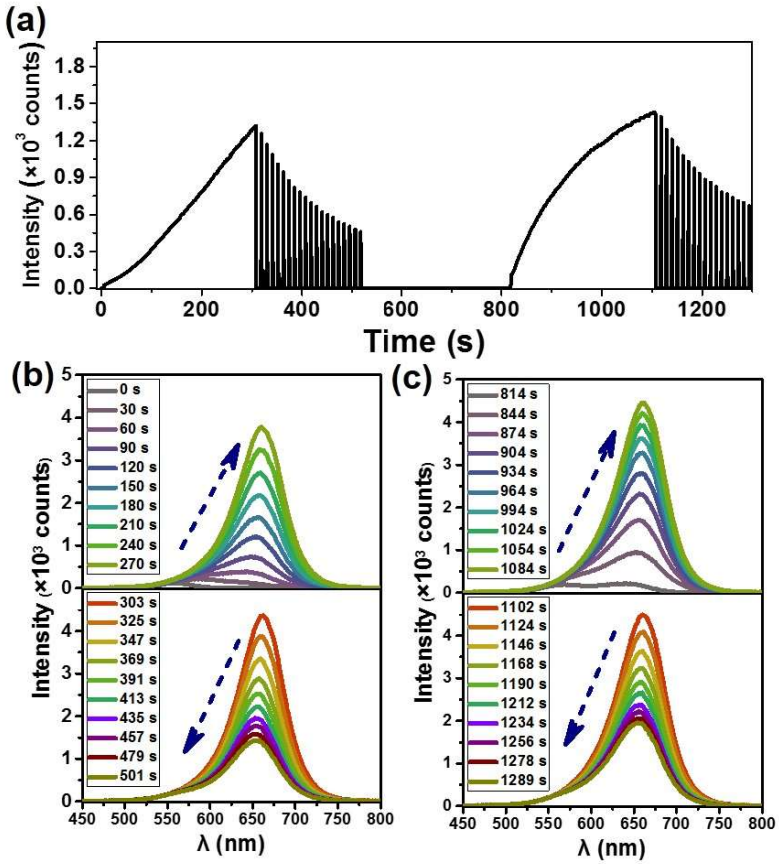

Figure S3. (a) PL traces of $CsPb_{0.9}Sn_{0.1}IBr_2$ film. The dark intervals were formed by turning off the excitation laser and then kept in dark for the durations of 10 s. (b, c) PL spectra of the PL traces measured in (a). The wavelength of the excitation laser is 450 nm, and the power density is 5 W/cm^2. The measurements were taken under N_2 atmosphere. Related to Figure 4.

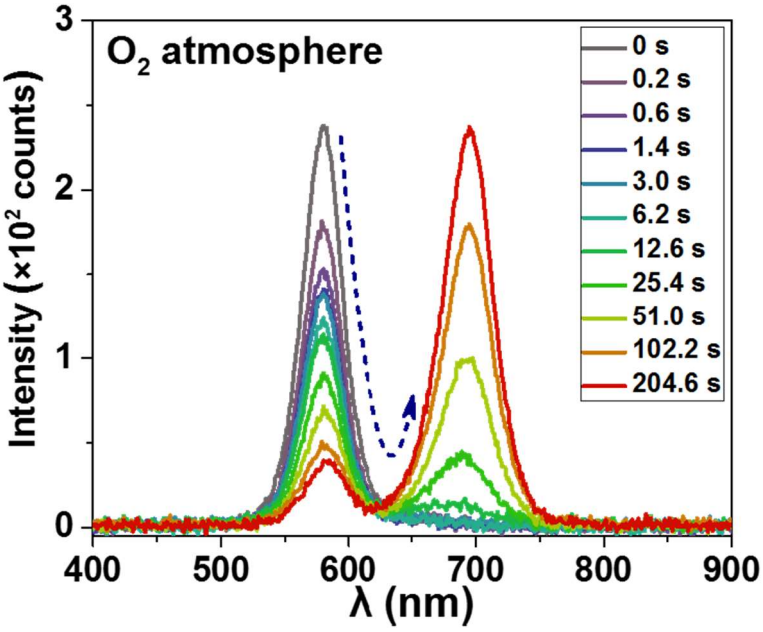

Figure S4. PL variations of $CsPbIBr_2$ film excited at 450 nm under oxygen atmosphere. The excitation power density is 5 W/cm^2. Related to Figure3 and Figure 5.

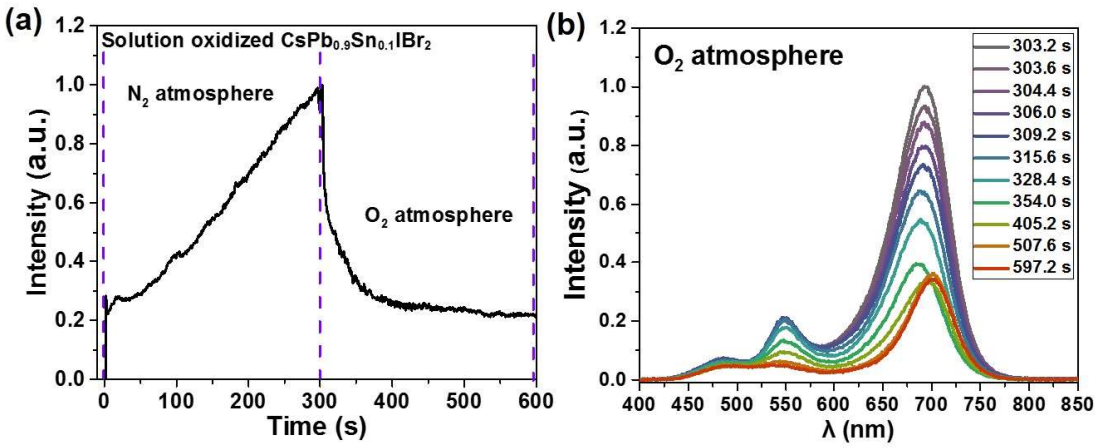

Figure S5. (a) PL traces of $CsPb_{0.9}Sn_{0.1}IBr_2$ film prepared by pre-oxidized precursor solution under different atmospheres. (b) PL spectra measured during the latter 300 s under oxygen atmosphere. The PL spectra variation measured during the first 300 s under nitrogen atmosphere has been shown in Figure 5b. Related to Figure 5.

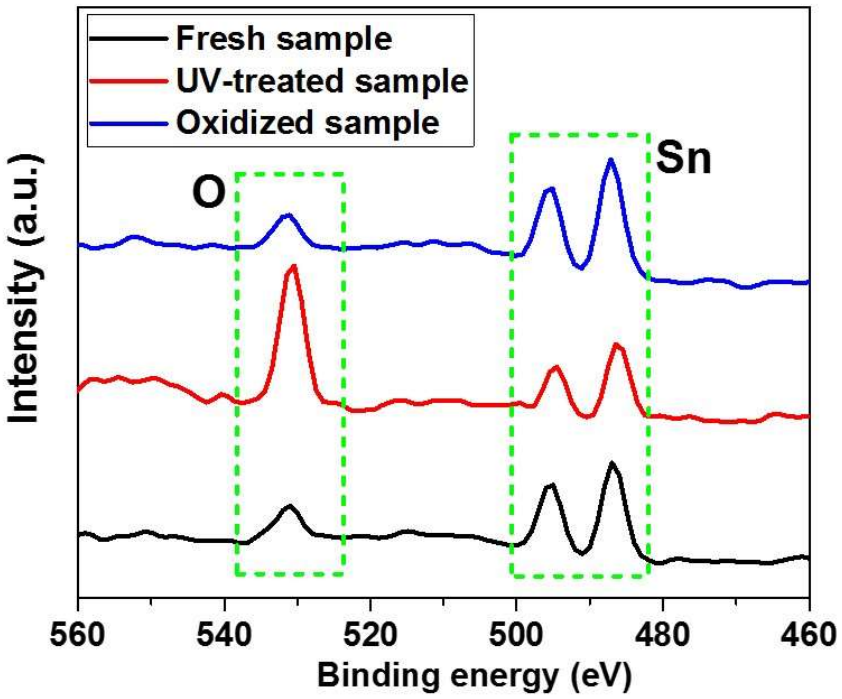

Figure S6. XPS spectra of $CsPb_{0.9}Sn_{0.1}IBr_2$ films pretreated via different ways. The fresh sample was prepared by fresh precursor solution; the UV-treated sample was prepared by fresh precursor solution and then treated under UV light in oxygen atmosphere for 30 min; the oxidized sample was prepared by pre-oxidized precursor solution. Related to Figure 5.

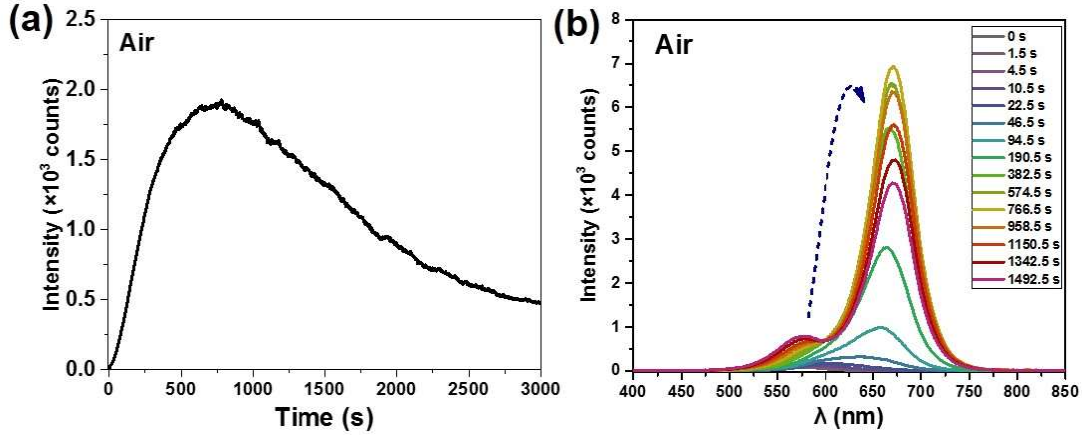

Figure S7. (a) PL traces of $CsPb_{0.9}Sn_{0.1}IBr_2$ film measured in humid air with a relative humidity of 40%. (b) The variation of PL spectra under continuous irradiation at 450 nm wavelength with an excitation power density of 5 W/cm^2. Related to Figure 6.

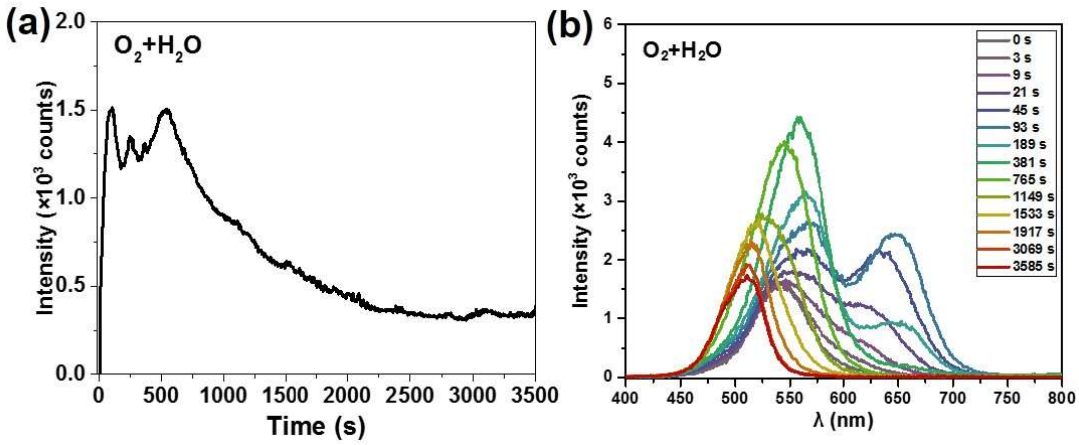

Figure S8. (a) PL traces of $CsPb_{0.9}Sn_{0.1}IBr_2$ film measured in the mixed atmosphere of oxygen and H_2O. (b) The variation of PL spectra under continuous irradiation at 450 nm wavelength with an excitation power density of 5 W/cm^2. Related to Figure 6.

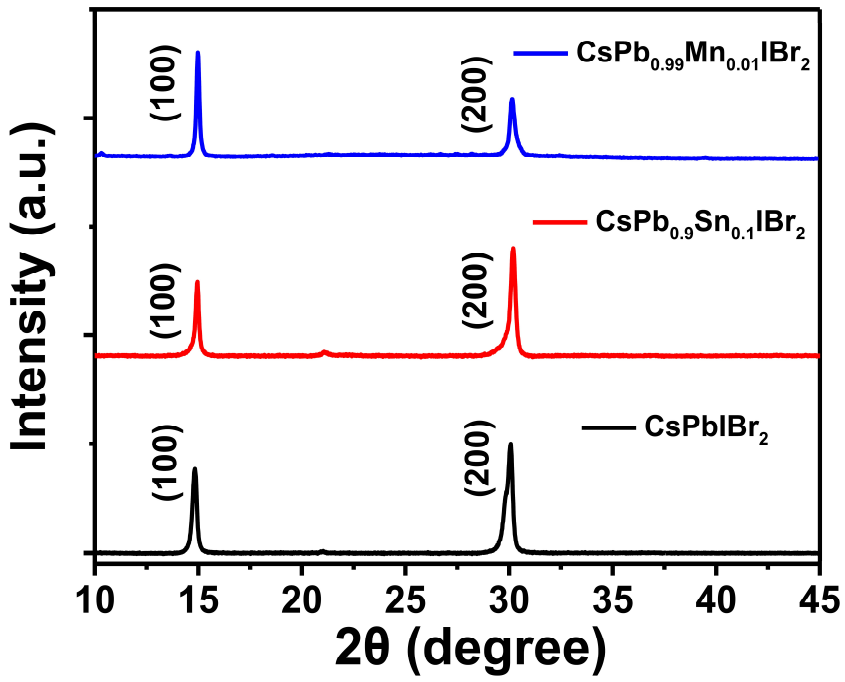

Figure S9. XRD spectra of $CsPbIBr_2$, $CsPb_{0.9}Sn_{0.1}IBr_2$, and $CsPb_{0.99}Mn_{0.01}IBr_2$ samples. Related to Figure 1 and Figure 6.

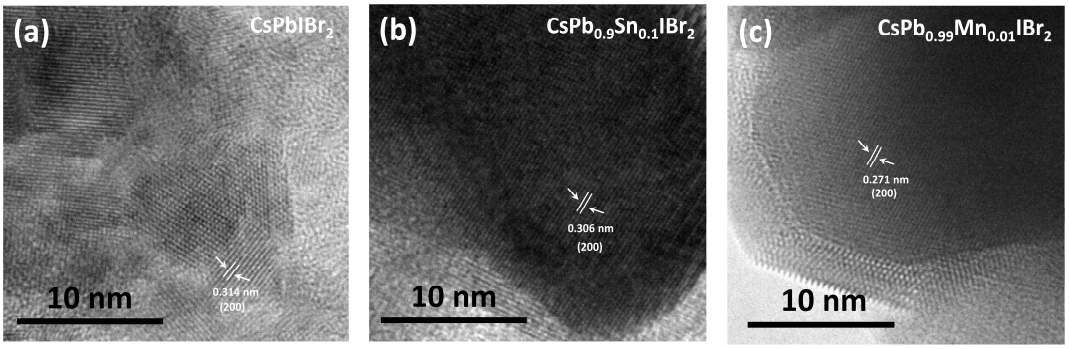

Figure S10. HR-TEM image of (a) $CsPbIBr_2$, (b) $CsPb_{0.9}Sn_{0.1}IBr_2$, and (c) $CsPb_{0.99}Mn_{0.01}IBr_2$. Related to Figure1 and Figure 6.

Tables:

Table S1. Quantitative analysis of the elemental contents in $CsPb_{0.9}Sn_{0.1}IBr_2$ film measured by EDX analysis. Related to Figure 1.

Element	***Wt %***	***At %***
CsL	17.05	16.29
PbL	37.01	22.68
SnL	1.58	1.7
IL	18.99	40.32
BrK	25.37	19.01
Matrix	Correction	ZAF

Transparent Methods:

Sample preparation: The $CsPb_{0.9}Sn_{0.1}IBr_2$ precursor solution was prepared by dissolving $PbBr_2$ (Aladdin, 99%) and $SnBr_2$ (Alfa Aesar, 99.2%) with a molar ratio of 0.9:0.1 in N,N-Dimethylformamide (DMF) under stirring for 30 min at 80 ℃ and then equimolar CsI (Aladdin, 99.999%) powder was added into the above mixture. The precursor solution was continuously stirred for 4 h at 80 ℃. After cooling to room temperature, the solution was filtered by a filtering membrane with 0.22 μm pore size (JinTeng, Nylon 66). The $CsPb_{0.99}Mn_{0.01}IBr_2$ solution was prepared by dissolving $PbBr_2$ (Aladdin, 99%) and $MnBr_2$ (Aladdin, 98%) with a molar ratio of 0.99:0.01 in DMSO under stirring for 30 min at 80 ℃ and then equimolar CsI (Aladdin, 99.999%) powder was added into the above mixture. The precursor was continuously stirred for 4 h at 80 ℃. The $CsPbI_{1.5}Br_{1.5}$, $CsPbI_{1.2}Br_{1.8}$ and $CsPbIBr_2$ solution was prepared by dissolving different molar ratios of $PbBr_2$ (Aladdin, 99%) and CsI (Aladdin, 99.999%) in DMF and stirred for 4 h at 80 ℃. The perovskite films studied in this work were prepared by spin-coating 50 μl of precursor solution on a cleaned glass coverslip under a rotation speed of 2500 rpm. The $CsPb_{0.9}Sn_{0.1}IBr_2$ precursor solutions were prepared under argon atmosphere, the $CsPb_{0.99}Mn_{0.01}IBr_2$, $CsPbI_{1.5}Br_{1.5}$, $CsPbI_{1.2}Br_{1.8}$ and $CsPbIBr_2$ precursor solutions were prepared under ambient atmosphere, and all of the perovskite films were prepared under ambient conditions.

Material characterizations： SEM and EDX characterizations were performed on a Hitachi S-4800 instrument. XRD measurements were carried out on a Shimadzu XRD-6000 powder X-ray diffractometer with a Cu *Kα* source (λ = 1.5418 Å) between 5-45° at a scanning rate of 5°/min. UV-vis spectra were recorded by an ultraviolet-visible spectrometer (UV-3600, Shimazdu). XPS analysis was performed on a PHI-5000 VersaProbe X-ray photoelectron spectrometer with an Al *Kα* X-ray source. The HR-TEM images of the perovskite were characterized by JEOL 2010F field-emission transmission electron microscope at 200 kV.

PL measurements： The PL spectra of the perovskite materials were analyzed by a home-built wide-field PL microscope. Briefly, a 450 nm diode CW laser was used as the excitation source and focused above the sample plane by a dry objective lens (Olympus LUCPlanFI 40×, NA=0.6). The luminescence light was collected by the same objective lens and detected by an EMCCD camera (Andor Ixon U888) after passing through a 473 nm long-pass filter (Thorlabs). The PL spectra were measured by putting a transmission grating (Newport, 150 lines/mm) in front of the camera. The atmosphere was controlled by purging the sample chamber with oxygen or nitrogen.